RSC Advances

ROYAL SOCIETY
OF CHEMISTRY

www.rsc.org/advances

Smart Excimer Fluorescence probe for visual Detection, Cell Imaging and

Extraction of Hg^{2+}

Syed S. Razi, Rashid Ali, Priyanka Srivastava and Arvind Misra*

Department of Chemistry, Faculty of Science, Banaras Hindu University, Varanasi – 221 005. UP INDIA.

Corresponding author: arvindmisra2003@yahoo.com; amisra@bhu.ac.in
Tel: +91-542-6702503; Fax: +91-0542-2368127, 2368175.

Abstract

Smart pyrene based simple fluorescent probes **2** and **4** were designed, synthesized and characterized by different spectroscopic methods. The photophysical properties of probes and their affinity towards different metal ions have been investigated in phosphate buffer. The molecular probes upon interaction with Hg^{2+} selectively, showed enhanced static excimer emission at 506 nm along with a naked-eye sensitive chromo and fluorogenic response. Probe **2** sensitively showed high limit of detection (3.4 *pM*) for Hg^{2+} in solution. The pyrene silicate derivative, **4** has been utilized to detect and extract Hg^{2+} in solution as well as solid state. The data obtained from NMR and ESI-MS spectroscopy supported about the mode of interaction in which the *N* and *O* atoms of –C=*N* and –OH functions of probe are involved to complex Hg^{2+} in 2:1 stoichiometry. Moreover, probe **2** has shown excellent selectivity for Hg^{2+} in protein medium (BSA/HSA) and was used to detect Hg^{2+} in live HeLa cells, on test paper strips and in real contaminated water samples.

Key Words: *Chemosensor, Hg^{2+}, Excimer, Organic scaffolds*

1

Introduction

Contemporary science researches have taken much interest to develop smart organic scaffolds/ fluorescent probes to detect biological and ecological important metal ions and anions through different photophysical mechanism.[1] Among the various detection methods, fluorescent chemosensors exhibiting ion-induced change in fluorescence behavior are attractive and advantageous in terms of sensitivity, selectivity, and response time.[2] Moreover, the development of sensitive and reliable molecular scaffolds and/or fluorescence "turn-on" sensors for heavy and transition metal ions (HTMs) are challenging due to the fluorescence quenching effect.[3] Also, the studies related to typical photophysical mechanisms of newly designed chemosensors such as, photoinduced electron transfer (PET), internal charge transfer (ICT), chelation enhanced fluorescence (CHEF), aggregation-induced emission (AIE), excimer, C=N isomerization etc.[4–8] are of continuing endeavor.

Recently, scientific community has found that contamination due to the heavy and transition metals (HTMs) brought forth serious environmental and health problems. Particularly, mercury (Hg^{2+}) is recognized as a detrimental neurological toxin which is widely distributed in the environment by various natural processes, industrial releases and anthropogenic activities. The bioaccumulation of such toxic material in living tissues of human and animal bodies via a food chain causes mercury poisoning, serious neural disorder and diseases like Minamata. [9-10] Environmental Protection Agency (EPA, USA) has set maximum allowable level of inorganic mercury in drinking water 2 ppb.[11]

In this direction, great efforts have been made to design efficient fluorescent molecular sensors[12-16] to detect Hg^{2+} either by fluorescence enhancement or quenching and color changes.[17] However, the numbers of good chemosensors to

detect Hg^{2+} through enhanced "*turn-on*" emission are limited in number. Because Hg^{2+} is known to induce fluorescence quenching due to the spin-orbit coupling effect/electron transfer mechanism and is spectroscopically and magnetically silent (closed shell d^{10} configuration).[18-20] Moreover, the poor aqueous medium compatibility of reeptors[19] also limits the application of such systems to work as a good analytical tool and/or sensitive sensor for Hg^{2+}.[21-27] Thus, the selective recognition and separation of traces of mercury in the environment and in real samples has great significance and worthy to investigate. Therefore, the development of cost-effective, sensitive and facile new synthetic small organic molecular scaffolds/chemosensors that are compatible in environment and biological milieus as well as in aqueous or partial aqueous medium, solid state and/or liquid–solid interface are important goals to provide instant optical feedback and online detection without involving sophisticated instrumentation.

Keeping these perspective in mind our ongoing research is currently paying attention toward development of some efficient fluorescent organic scaffolds/motifs to detect cations, anions, and biomolecules sensitively in different medium.[8] Through this contribution we present design, synthesis and potential application of pyrene based two very simple smart potential fluorescent probes, **2** and **4** to detect and extract Hg^{2+} in partial aqueous medium and on solid support surfaces. We assumed that the donor sites of the probes, available in the form of *N* and *O* atoms, would show high affinity for a soft closed-shell cation, Hg^{2+} and form stable complexation in the medium.[28] Also, the introduction of ethanolamine moiety would help to generate a stable minimum energy configuration to work on the excimer mechanism.[10-11] To accomplish the objective of solid state chemosensing as well as mercury extraction from solution we strategies a methodology on conventional silica gel polymer

material. The high fluorescence "turn-on" chemodetection sensitivity displayed by a solid chemosensory material **4** is interesting and provided an additional way to extract and detect Hg^{2+} in different medium. Moreover, the sensitivity of probe to detect Hg^{2+} selectively in real water sample, on cellulose paper strips, in protein medium (BSA and human HSA) as well as in live HeLa cells through excellent fluorescence turn-on response suggested their promising prospect in environmental and biological science.

Experimental

Synthesis of probes and General experimental procedures: Data related to synthesis and characterization of probes and general experiment methodology are provided in supplementary information file (ESI).

Results and Discussion

Probe Design, photophysical behavior and metal ion selectivity:

Recently, some immobilized modified fluoroionophore on the surface of alumina or silica and nano materials have been explored to detect HTMs.[8] Interestingly, the use of silica gel offers amorphous inorganic polymer surface with abundance of siloxane (Si–O–Si) and silanol (Si–OH) functions in the bulk and on the surface, respectively. The silanol function present on the surface may be easily explored to introduce chemical modifications, tether group and incorporate modified fluoroionophore to trap and/or extract metal ions reversibly. Consequently, the variations in the specific optical behavior in a particular sensing event are easy to follow by different spectroscopic methods. The signaling fluorophore unit like, pyrene is known for good quantum yield and chemical stability.[9] It shows characteristic monomer emission at 370 – 410 nm and typical excimer emission between 470 to 520 nm due to the formation of an excited state dimer at a low electronic energy state.[10]

4

The excimer emission of pyrene is tunable and can be easily utilized to detect sensitively the guest species[11] like a molecular *OFF-ON* switch.[20]

Scheme 1 describes the synthetic route for molecular probes **2** and **4**. Pyrene carboxaldehyde and ethanolamine were refluxed in ethanol to obtain a solid yellow colored compound **2** in good yield (78%). Compound **2** in the presence of diiospropylethylamine was reacted with 3-chloropropyltriethoxysilane in dry dichloromethane to get compound **3** in 72% yield. Compound **3** and silica gel (particle size, 75–150 μm; average pore diameter 25–30Å) were stirred overnight at room temperature in dry dichloromethane to obtained probe **4** as an orange color solid in 68% yield. The isolated compounds were characterized by different spectroscopic techniques and data are included as supplementary material (Figure S1-8).

"Scheme – 1"

The photophysical behavior of probe **2** has been examined through the absorption and emission spectroscopy at room temperature in phosphate buffer (10 mM pH 7.0; 10% aqueous ACN). The absorption spectrum of **2** (10 μM) displayed low and high energy absorption bands at 357 nm (ε = 7.26 x 10^4 $M^{-1}cm^{-1}$) and 284 nm (ε = 6.69 x 10^4 $M^{-1}cm^{-1}$) respectively, along with shoulder at 386, 342 and 273 nm. Upon excitation at 345 nm **2** (10 μM) displayed typical pyrene monomer emission at 375, 393 and 414 nm (Φ_2 = 0.004) (Figure 1). The affinity of probe **2** toward different metal ions (2.0 equiv) such as, Na^+, K^+, Ca^{2+},Mg^{2+}, Co^{2+}, Ni^{2+}, Cu^{2+}, Zn^{2+}, Al^{3+}, Fe^{2+}, Fe^{3+}, Pb^{2+}, Ag^+, Cd^{2+}, and Hg^{2+} (as their nitrate salts) have been examined in phosphate buffer. Notably, the absorption maxima of **2** upon interaction with Hg^{2+} and Cu^{2+} ions showed considerable bathochromic shift (~78 nm) and a new electronic transition band appeared at ~ 435 nm (**2**+Hg^{2+}; ε = 4.07 x 10^4; **2**+Cu^{2+}; ε =1.19 x 10^4

M^{-1} cm^{-1}) (Figure 1, inset) and a naked eye sensitive green color appeared in the medium (Figure 2). Similarly, upon interaction with Hg^{2+} and Cu^{2+} probe **2** exhibited enhanced excimer emission, "turn-on" at ~ 506 nm (red shift, ~113 nm) in which, relative emission intensity enhanced with ~ 10 fold (Φ_{2+Hg}^{2+} = 0.039) and ~ 1.5 fold (Φ_{2+Cu}^{2+} = 0.086) increase in quantum yield, respectively (Figure 1). The color of solution changed from a fluorescent blue to a naked-eye sensitive bright fluorescent cyan color under UV light (at 365 nm) (Figure 2). The other tested metal ions revealed insignificant change in the absorption and emission spectra of probe.

Further, with competitive metal ions interference studies have been performed to understand the high affinity of **2** for Hg^{2+}. Interestingly, upon a sequential addition of tested metal ions (in excess, 20 equiv) to a solution of probable complex, **2**+Hg^{2+} or reversibly, addition of Hg^{2+} to a solution of **2**+M^{n+} ions (Figure S9) insignificant changes were observed in the relative emission intensity and the color of a complex, **2**+Hg^{2+} (Figure S10). Moreover, the reversible mode of complexation could be realized by the addition of a strong chelating reagent, EDTA to a solution of probable complex, **2**-Hg^{2+}. Notably, the observed revived emission was almost close to the monomer emission of **2** due to strong binding affinity of EDTA with Hg^{2+}.[10] Reversibly, upon addition of Hg^{2+} to a solution of probe **2** containing EDTA no excimer emission was observed. This process was repeated successfully for ten times and in every cycle probe **2** behaved almost consistently (Figure S11). Thus, it is noteworthy to mention that **2** upon complexation with Hg^{2+} and/or Cu^{2+} through the coordination sites available in form of *O* and *N* atoms of hydroxyl and aldimine functions and form a stable dimeric species in the medium in which two pyrene units acquired stacked conformation due to enhance $\pi \rightarrow \pi$ electrostatic interaction.[29]

6

"Figure – 1 and 2"

Moreover, it is well known that if a fluorescent probe and/or its complex, upon excitation at their emission maxima do not show complete spectral overlap, the observed enhanced fluorescence may be assigned to static excimer emission.[10] Therefore, to ensure that the observed enhanced emission upon complexation of probe **2** with Hg^{2+} is due to either static or dynamic excimer formation the fluorescence excitation spectra were acquired (Figure S12). Probe **2** and its probable complex, **2**-Hg^{2+} were excited corresponding to their observed monomer and excimer emission maxima centered, at 397 and 506 nm, respectively. Interestingly, the probable complex, **2**-Hg^{2+} displayed new emission bands at ~ 445 and 558 nm while no such emission was observed when probe **2** was excited at 397 and 506 nm respectively. Thus, the observations clearly supported about the survival of static excimer emission which is well induced by the Hg^{2+} in the present sensing event.

The absorption and emission titration studies have been performed to understand the binding affinity of **2** (10 μM) with Hg^{2+}. Upon a gradual addition of Hg^{2+} (0–2 equiv) to a solution of **2** the absorption bands centered, at 357, 284 and 248 nm reduced progressively and new bands appeared at 435 (ε = 4.18 x 10^4 $M^{-1}cm^{-1}$), 301 (ε = 3.5 x 10^4 $M^{-1}cm^{-1}$), 258 (ε = 3.82 x 10^4 $M^{-1}cm^{-1}$) and 232 (ε = 1.01 x 10^4 $M^{-1}cm^{-1}$) nm (Figure 3). The formation of multiple isosbestic points at 372 nm, 316, 287, 267, 254 and 237 nm suggested about the existence of more than one species in medium probably, the dimeric complex, complex, **2**+Hg^{2+} and also the geometrical change in the structure of the probe from *E* to *Z* isomer. Similarly, the acquired emission titration spectra of **2** displayed a gradual decrease in the monomer emission (at 393 nm) while the intensity of a new excimer emission enhanced (~ 5 fold) continuously at 506 nm (red shift of ~ 113 nm) (Figure 3). The estimated quantum yield was found

to increase about ~ 10 fold ($\Phi_{2+Hg}{}^{2+}$= 0.039). Job's plot analysis revealed consistently a 2:1 binding stoichiometry for an interaction between **2** and Hg^{2+} ions (Figure S13). For which the association constants were estimated by B-H method[30] and were found to be K_{abs} = 7.29 x 10^3 and K_{em} = 2.28 x 10^4 /$M^{1/2}$ respectively (Figure 3, insets).

"Figure – 3"

The pH dependence of probe 2:

The pH dependent photophysical behavior of probe **2** and its probable complex, **2**+Hg^{2+} were examined in phosphate buffer (Figure 4 and S14). The optical behavior of probe **2** was found insensitive in the pH range 5.5 to 14. However, in acidic medium (pH,< 5.5) the absorption spectra showed red shift of ~79 nm and a new band appeared at 437 nm (Figure S14a) however, the observed enhanced emission was almost close to the excimer emission (Figure 4 and S14b). Moreover, the ratio of monomer to excimer emission (I_E/I_M) as a function of pH markedly decreased from pH 6 while almost negligible change occurred at very high and low pHs. It is noteworthy to mention that the hydrophobic association between the alkyl chains play important role in determining the overall electrostatic interaction and self aggragation.[31] Thus, due to variable interaction, the possibility for the existence of different type of excimer in the medium cannot be ignored. Additionally, the pH dependent photophysical response of a complex, **2**+Hg^{2+} was examined and found almost constant in the range of pH 4 to 9. At high pH (≥ 9) an abrupt decrease in relative emission intensity could be reasoned to dissociation of complex, **2**+Hg^{2+}.[28] Thus, the fluorescence response of **2** can be utilized in pH range 5.25−8.93 within which most of the biological samples can be tested.

"Figure – 4"

Limit of detection of probe 2

In order to estimate the limit of detection (LOD) for probe **2** calibration curve has been acquired as done previously.[28] An almost linear calibration curve gave the standard deviation (σ) 0.23172 (Figure - 5a). Similarly, from the slope of fluorescence plot obtained by the change in relative fluorescence intensities ΔI $(I - I_0)$ with respect to different concentration of Hg^{2+} $(10^{-4}$ μM) gave the calibration sensitivity (m) 20.633 (Figure 5). The limit of detection (LOD) was estimated using Eq. (3) and was found to be 3.4 *pM* which is good and comparable to other reported methods.[28]

<div align="center">**"Figure – 5"**</div>

Mechanism of Complexation between 2 and Hg^{2+}

To have an insight about the mode of interaction ^{1}H NMR, FT-IR and HRMS spectra of probe **2** and a complex, **2**+Hg^{2+} were analyzed. ^{1}HNMR spectrum of **2** showed resonances corresponding to pyrene ring protons as multiplet at δ 8.36-8.08 ppm (H4, H6, H7, H8 and H10, H11, H13) while doublet appeared at δ 9.12 and 8.56 ppm are attributable to H3 and H14 protons, respectively (Figure 6, S1). Similarly, the resonances appeared as singlet and doublet at δ 3.79, 3.87 and 9.34 ppm have been assigned to H3', H4' (-CH₂) and aldimine (-CH=N), H1' protons, respectively. The resonance corresponding to OH function proton appeared at δ 4.73 ppm. In contrast, the ^{1}HNMR spectra of a probable complex, **2**+Hg^{2+} exhibited significant downfield shift corresponding to resonances of H1' (Δδ = 1.46), H3 (Δδ = 0.47), H14 (Δδ = 0.43), pyrene unit (Δδ = 0.56 ppm) and H3' (Δδ = 0.18) protons. Similarly, the -OH proton resonances shifted downfield and become broadened to appear at δ 4.79 ppm (Δδ = 0.57 ppm) while the H4' proton shifted upfield (Δδ = 0.04 ppm) to appear at δ 3.83 ppm (Figure S15-17). Moreover, the FT-IR spectrum of **2** showed characteristic stretching vibration bands at 3439, 2943, 1631, 1077 cm⁻¹ corresponding to, -OH, -

CH, -C=N, and -CO functions, respectively (Figure S18). Upon interaction with Hg^{2+} the OH stretching vibration disappeared almost completely, and -C=N stretching vibration revealed blue shift and appeared at 1617 cm^{-1}. In mass (HRMS) spectra the molecular ion peak, at m/z^+ 273.1156 (calc. 273.1153) for probe **2** upon complexation with Hg^{2+} appeared at m/z^+ 870.8308 (calc. 870.8306) (Figure S5 and S19). Thus, the observed spectroscopy data clearly supported about the interaction of probe **2** with Hg^{2+} through the *O* and *N* atoms of hydroxyl and aldimine functions in 2:1 stoichiometry, along with geometrical change in the structure of probe **2** from *E* to *Z* isomer[32] as predicted in scheme – 2.

"Figure – 6" and "Scheme – 2"

Quantum Chemical calculations

To have a better understanding of the binding mode and optical response of 2 toward Hg^{2+}, energy optimization and frequency calculations were performed on **2** and its complex, **2**+Hg^{2+}. Quantum chemical calculations were performed at the B3LYP density functional theory (DFT) level using B3LYP/6-31G(d,p) for **2** and B3LYP/LANL2DZ for the **2**+Hg^{2+} complex. All the frequency calculation and geometry optimizations was performed in Gaussian 03 program suite[33] to make sure that the optimized structure is a real minimum. DFT optimized structure revealed two bond lengths between Hg^{2+} and *N* atom of aldimine function at 2.45Å and 2.65Å while between Hg^{2+} and *O* atom of hydroxyl function at 1.92Å respectively. The optimized structure of **2**-Hg^{2+} complex (Figure 7) suggested that Hg^{2+} coordinated with *N* and *O* donor atoms **2** in octahedral geometry.

"Figure – 7 and"

Optoelectronic behavior of probe 4:

To accomplish the goal of solid state chemosensing and extraction of mercury in real samples, a reusable sensory material was successfully prepared by immobilizing modified probe **2** on to the surface of mesoporous silica gel by sol–gel method.[34] Due to strong affinity between functional triethoxysilyl and silanol units the immobilization of probe **2** on the silica gel surface occurred successfully through silyl-etheral (–Si–O–Si–) linkages.[35] The yellow–orange colored mesoporous solid chemosensing probe, **4** was characterized by FT-IR AFM and SEM spectral data. The FT-IR spectrum (Figure S8) of **4** with respect to free silica gel exhibited aliphatic and aromatic (C–H and C=C) stretching vibration bands at 3167, 2925, and 1444 cm^{-1} respectively while the broad stretching vibration band due to OH function, at 3444 cm^{-1} disappeared completely. The appearance of typical –Si–O–Si– and -C=N stretching vibration bands at 1089 and 1644 cm^{-1} respectively, provided a solid evidence for the attachment of **2** on to the mesoporous silica surface.

<p style="text-align:center">**"Figure – 8"**</p>

To have an idea about the aggregation and its effect on optical behavior of probe the solution of **4** in methanol were subjected to scanning electron (SEM) and atomic force (AFM) microscopy, before and after addition of Hg^{2+} ions. The SEM images, as shown in Figure 8a,b (Figure S20) have given an idea about the inconsistent pattern of silica gel particles with an average diameter of 20 μm. This could be probably attributed to the formation of different types of aggregates on the surface. Moreover, when the images of Hg^{2+} treated probe was acquired the average particle size was substantially reduced to ∼ 10 μm (Figure 8b). This has suggested about the Hg^{2+} induced enhanced aggregation and roughness in comparison to unmodified silica-gel polymeric material (Figure 8a, b and Figure S21). Thus, the change in macroscopic properties due to morphological variation resulted the changes in color of the silicate

material from an orange red to yellow-green color which, also indicated about the

attachment of probe to the surface of silica gel (Figure 9). Also, the shape and size of

these aggregates are in good agreement with the data obtained from AFM

measurements in which the average root mean square roughness of **4** and peak to

valley height area were found to be 2.077 and 1.507 nm, respectively (Figure 8). The

mechanism of aggregate build-up has been deduced considering the dominance of the

solid state interactions in the aggregated state which has been evidenced further by

powder XRD pattern (Figure 8c). Thus, the modified and aggregated rough surfaces

of **4** make it a suitable potential solid material to detect and extract Hg^{2+} from the

contaminated solution and the environment.

<div align="center">**"Figure – 9"**</div>

Selectivity of probe 4 with metal ions:

The optoelectronic behavior of sol solution of **4** has been examined in the absence

and presence of tested metal ions in phosphate buffer (10 mM pH 7.0; 10% aqueous

ACN). Interestingly, the optoelectronic behavior of **4** was found almost consistent to

probe **2.** The characteristic low and high energy, $\pi \rightarrow \pi^*$ electronic transition bands

appeared at 393 nm ($\varepsilon = 27,000$ $M^{-1}cm^{-1}$), 360 nm ($\varepsilon = 35,400$ $M^{-1}cm^{-1}$) and 286 nm (ε

$= 52,000$ $M^{-1}cm^{-1}$) respectively (Figure 10). Upon excitation at 360 nm probe **4**

displayed broad weak monomer emission at 390 and 413 nm. Next we examined the

affinity of **4** for tested metal ions (2.0 equiv). Probe **4** high sensitivity and selectivity

for Hg^{2+} in which absorption band centered, at 286 nm exhibited large hyperchromic

shift while the band centered, at 360 nm displayed a blue-shift of ~3 nm ($\lambda_{max} = 357$

nm; $\varepsilon = 41,600$ $M^{-1}cm^{-1}$). Similarly, upon interaction with Hg^{2+} probe **4** (at $\lambda_{ex} = 360$

nm**)** exhibited enhanced excimer emission at 502 nm (Figure 10). While the other

tested metal ions failed to exhibit any significant change in the optical behavior of

probe. Moreover, the competitive metal ion interference studies also suggested about the high selectivity of **4** for Hg^{2+} ions (Figure S22). The jobs plot analysis revealed consistently a 2:1 stoichiometry for an interaction between **4** and Hg^{2+} ions for which binding constants have been estimated through the absorption and emission titration experiment data, and were found to be $K_{ass.(abs)} = 3.60 \times 10^6 /M^{1/2}$ (Figure S23c) and $K_{ass.(em.)} = 2.5 \times 10^5 /M^{1/2}$ respectively (Figure S23d).

Next we tried to acquire the emission spectra of **4** in solid state. In solid state probe **4** upon excitation at $\lambda_{ex} = 345$ nm showed broad weak monomer emission at 385 and 410 nm. Upon interaction with Hg^{2+} probe **4** showed a noticeable enhanced emission at $\sim$ 510-540 nm and the color of silica derived probe was changed from a naked-eye sensitive orange red to yellow-green color (Figure 10). Additionally, when **4** was treated with EDTA solution the monomer emission revived. This process was repeated five times and intensity was found almost constant. Thus, it is noteworthy to mention that solid material **4** may be practically explored further as a reusable solid fluorescent chemosensor/optoelectronic material to detect and extract the Hg^{2+} in the environment.

<p align="center">**"Figure – 10"**</p>

Affinity of probe 2 to detect Hg^{2+} in Biological medium:

The potential applicability of probe **2** to detect Hg^{2+} in a biological medium such as, a blood plasma protein BSA (bovine serum albumin) and HSA (human serum albumin) has also been studied. We previously observed[28] that Hg^{2+} quenches ($\sim$83%) the typical inherent emission of BSA ($\lambda_{em} = \sim$ 345 nm) (Figure S24). Therefore, to understand the possibilities of nonbonding interaction we first investigated photophysical behavior of **2** in the presence of BSA and HSA in phosphate buffer. Interestingly, the emission behavior of **2** at 345 nm excitation remained independent

to the even high concentration of BSA/HSA (0 - 2 µM) (Figure S25a). Thus, suggesting that the photophysical behavior of probe **2** in protein medium does not get effected due to possible H-bonding and/or electrostatic interactions as well as by the interaction of different kind of electrolytes present in blood serum. Therefore, we examined the affinity of **2** to detect Hg^{2+} in the protein medium. It is important to mention that in the presence of BSA and HSA (2 µM BSA/HSA, phosphate buffer pH 7.0) probe **2** (10 µM) upon interaction with Hg^{2+} (2.0 equiv), showed considerable enhanced (~75%) emission at ~ 506 nm (Figure 11, and S25b) and readily detectable naked-eye sensitive weak fluorescent blue color of solution (*turn–Off*) changed to a bright fluorescent blue-green color (*turn–On*) (Figure 11b inset). The usability of **2** to determine Hg^{2+} in biological samples was assessed by emission titration experiment. The emission titration pattern displayed by **2** in human blood serum was found consistent to the behavior observed in aqueous solution (Figure 11b). In human blood serum the limit of detection for Hg^{2+} has been estimated as above and was found to be 0.02 µM (4.31 ppb) (Figure S26). Thus it is worth to mention that probe **2** can be utilized as a potential chemosensor to detect Hg^{2+} in biological samples.

"Figure – 11"

Detection of Hg^{2+} in Living Cells:

The good response of probe **2** to detect Hg^{2+} smartly in protein medium prompted us to study the feasibility of **2** *in vivo* to detect Hg^{2+} in live cells through confocal fluorescence microscopy. As done previously,[36] HeLa cells were first incubated directly with different concentrations (10, 20, 30, 40, 50 µM) of **2** and after proper washing (5 min, two times) with phosphate buffer (1X PBS saline, pH 7.4) cells were visualized under the microscope. The observed bright blue color fluorescence indicated excellent cell permeability of **2** in HeLa cells (Figure 12). Moreover, to

understand cell viability and cytotoxic tolerance of HeLa cells MTT assay was performed[36] corresponding to probe **2** and its complex, **2**+Hg^{2+}. MTT assay experiment implicated that more than 50% cells were viable up to 30μM concentration of probe **2** and its complex, **2**+Hg^{2+}. Therefore, 30 μM concentration of probe **2** and **2**+Hg^{2+} was chosen as an optimum concentration to incubate HeLa cells separately in dark. The confocal microscopic images of HeLa cells (at λ_{ex} = 380 nm) illustrated intense enhanced green fluorescence for **2**+Hg^{2+} (Figure 12, images D, E and F). Thus, the cell imaging experiment suggest the potential application of probe **2** to detect Hg^{2+} in live cells.

<p style="text-align:center">**"Figure – 12"**</p>

Analytical Applications

Detection of Hg^{2+} on cellulose Strip kit

In order to make sure the analytical use of probe **2** paper strip test was performed. Small cellulose paper strips (Whatman^{TM}) containing different concentration of probe **2** (5, 3, and 1 μM) were prepared (1.5 × 2.0 cm^2) in 10% aqueous ACN and dried in air. The aqueous Hg(NO$_3$)$_2$ solution of three different concentrations, 1×10^{-5}, 1×10^{-7}, and 1×10^{-9} M were prepared and dried test paper strips were dipped in for 10 min. The observed fluorescent green color of air dried paper strips under UV light (at 365 nm) demonstrated the potential application of probe **2** to detect Hg^{2+} on the solid surface (Figure 13).

<p style="text-align:center">**"Figure – 13"**</p>

Detection of Hg^{2+} in solid state and in real contaminated water samples:

To validate practical analytical utility of probe **2** and **4** to determine the Hg^{2+} concentration in real contaminated water samples we first quantified the fluorescence of probe **2** and **4** (10 μM) in the presence of various concentrations of Hg^{2+} ions (0 – 5 μM) and the corresponding calibration plots were prepared as the standard curves

(Figure 14a and 14b). Considering the possible interference that other components may cause in real samples the level of Hg^{2+} in real water samples was determined using the standard addition method.[28] Prior to real sample detection, when probe **2** and **4** were added directly to the water samples, no significant fluorescence enhancement occurred. However, when the emission spectra of treated contaminated water samples were acquired by this method the recovery of Hg^{2+} with respect to standard calibration curve was excellent. Notably, we could quantify Hg^{2+} contamination in real water samples in the range of 116 to 92% (Table 1 and 2). Moreover, the color of solutions also changed from a fluorescent blue to a blue-green which was readily visual to the naked-eyes (Figure 14a and 14b inset).

<div align="center">

"Figure - 14"

"Table – 1 and 2"

</div>

Conclusion

In conclusion, a novel pyrene based fluorescent probe has been designed and synthesized to detect Hg^{2+} sensitively and selectively in partial aqueous medium, biological medium as well as in solid state through fluorescence *turn-on* response. The interaction of Hg^{2+} with the aldimine and hydroxy fragments results excimer formation in which the two pyrene rings acquired stacked arrangements to enhance π – π interaction, and consequently enhanced emission was observed. Moreover, the non-fluorescent color of solution was changed to a fluorescent blue green which was readily visual to the naked eyes. The application of probe to detect Hg^{2+} in human blood serum, live cells, and test paper strip and in real water sample suggested promising prospect of Hg^{2+} sensing in biological medium and environment. The present methodology also provides a strategy to detect and extract traces of Hg^{2+} in solid state by the use of reusable mesoporous supramolecular aggregates.

ASSOCIATED CONTENT

Supporting Information. Synthesis**,** Experimental details, ^{1}HNMR, ^{13}CNMR, FT-IR, ESI-MS, HRMS, UV-Vis and fluorescence spectra.

AUTHOR INFORMATION

Corresponding Author

E-mail: arvindmisra2003@yahoo.com. amisra@bhu.ac.in.

Notes

Authors declare no competing financial interest.

References:

(1) J. Wu, W. Liu, J. Ge, H. Zhang, P. Wang, *Chem. Soc. Rev.,* 2011, 40, 3483–3495.

(2) A. K. Dwivedi, G. Saikia, P. K. Iyer, *J. Mater. Chem.,* 2011, 21, 2502–2507.

(3) X. Lou, Ou, D. D. Q. Li, Z. Li, *Chem. Commun*., 2012, 48, 8462–8477.

(4) G. Aragay, J. Pons, A. Merkoci, *Chem. Rev.,* 2011, 111, 3433–3458.

(5) M. Sauer, *Angew. Chem., Int. Ed.,* 2003, 42, 1790–1793.

(6) K. Hanaoka, Y. Muramatsu, Y. Urano, T. Terai, T. Nagano, *Chem. Eur. J.,* 2010, 16, 568–572.

(7) M. Mameli, M. C. Aragoni, M. Arca, C. Caltagirone, F. Demartin, G. Farruggia, G. D. Filippo, F. A. Devillanova, A. Garau, F. Isaia, V. Lippolis, S. Murgia, L. Prodi, A. Pintus, N. Zaccheroni, *Chem. Eur. J.,* 2010, 16, 919–930.

(8) J. Yin, Y. Hu, J. Yoon, *Chem. Soc. Rev.,* 2015, 44, 4619-4644.

(9) A. W. Czarnik, ACS symposium series 538, pp 235: Washington, D.C. 1992.

(10) A. P. deSilva, D. B. Fox, A. J. M. Huxley, T. S. Moody, *Coord. Chem. Rev.,* 2000, 205, 41-57.

(11) E. M. Nolan, S. J. Lippard, *Chem. Rev.,* 2008, 108, 3443–3480.

(12) X. Chen, T. Pradhan, F. Wang, J. S. Kim, J. Yoon, *Chem. Rev.,* 2012, 112, 1910–1956.

(13) J. Wang, X. Qian, *Chem. Commun.,* 2006, 109-111.

(14) S. Yoon, A. E. Albers, A. P. Wong, C. Chang, *J. Am. Chem. Soc.,* 2005, 127, 16030-16031.

(15) A. Ono, H. Togashi, *Angew. Chem., Int. Ed.,* 2004, 43, 4300- 4302.

(16) P. Chen, C. A. He, *J. Am. Chem. Soc.,* 2004, 126, 728-729.

(17) M. Hollenstein, C. Hipolito, C. Lam, D. Dietrich, D. M. Perrin, *Angew. Chem. Int. Ed.,* 2008, 47, 4346– 4350.

(18) T. J. Dickerson, N. N. Reed, J. J. LaClair, K. D. Janda, *J. Am. Chem. Soc.,* 2004, 126, 16582-16586.

 (19) J. Y. Kwon, Y. J. Jang, Y. J. Lee, K. M. Kim, M. S. Seo, W. Namand, J. Yoon, *J. Am. Chem. Soc.,* 2005, 127, 10107-10111.

(20) G.-K. Li, Z.-X. Xu, C.-F. Chen, Z.T. Huang, *Chem. Commun.,* 2008, 1774-1776.

(21) M. J. V. Ros-Lis, D. Marcos, R. Martinez-Manez, K. Rurack, J. Soto, *Angew. Chem., Int. Ed.,* 2005, 44, 4405-4407.

(22) J. Ding, H. Li, C. Wang, J. Yang, Y. Xie, Q. Peng, Q. Li, Z. Li, *ACS Appl. Mater. Interfaces*, 2015, **7**, 11369−11376.

(23) Y.-R. Zhang, Q.-R. Wang, P. Su, F. Zhao, J. Huanga, B.-X. Zhao, *RSC Adv.*, 2015, 5, 20634–20638.

(24) Y. Xua, Z. Jiang, Y. Xiao, T.-T. Zhang, J.-Y. Miao, B.-X. Zhao, *Analytica Chimica Acta*, 2014, 807, 126– 134.

(25) W.-Y. Liu, S.-L. Shen, H.-Y. Li, J.-Y. Miao, B.-X. Zhao, *Analytica Chimica Acta*, 2013, 791, 65– 71.

(26) Y. Zhang, Y. Yang, J. Hao, C. Yin, F. Huo, J. Chao, D. Liu, *Spectrochimica Acta Part A: Molecular and Biomolecular Spectroscopy*, 2014, 132, 27–31.

(27) F.-J. Huo, Y.-Q. Sun, J. Su, Y.-T. Yang, C.-X. Yin, J.-B. Chao, *Org. Lett.*, 2010, 12, 4756-4759.

(28) P. Srivastava, S. S. Razi, R. Ali, R. C. Gupta, S. S. Yadav, G. Narayan, A. Misra, *Anal. Chem.,* 2014, 86, 8693−8699.

(29) M. Shahid, S. S. Razi, P. Srivastava, R. Ali, B. Maiti, A. Misra, *Tetrahedron,* 2012, 44, 9076-9084.

(30) H. A. Benesi, J. H. Hildebrand, *J. Am. Chem. Soc.,* 1949, 71, 2703-2707.

(31) T. Joy, Kunjappu, P. Somasundara, *Langmuir.,* 1995, 11, 428-432.

(32) Y. Saito, K. Matsumoto, Y. Takeuchi, S. S. Bag, S. Kodate, T. Morii, I. Saito, *Tetrahedron Letters*., 2009, 50, 1403–1406.

(33) M. J. Frisch, G. W. Truncks, H. B. Schlegel, GAUSSIAN 03, Revision, E.01 Gaussian Inc., Wallingford CT 2007.

(34) Z. Sun, D. Guo, L. Zhang, H. Li, B. Yang, S. Yan, *J. Mater. Chem. B*, 2015, 3, 3201-3210.

(35) Y. Chen, C. L. Droumaguet, K. Li, W. E. Cotham, N. Lee, M. Walla, Q. Wang, *J. Am. Soc. Mass Spectrom.,* 2010, 21, 403–410.

(36) P. Srivastava, S. S. Razi, R. Ali, S. Srivastav, S. Patnaik, S. Srikrishna, A. Misra, *Biosensors and Bioelectronics,* 2015, 69, 179-185.

RSC Advances Accepted Manuscript
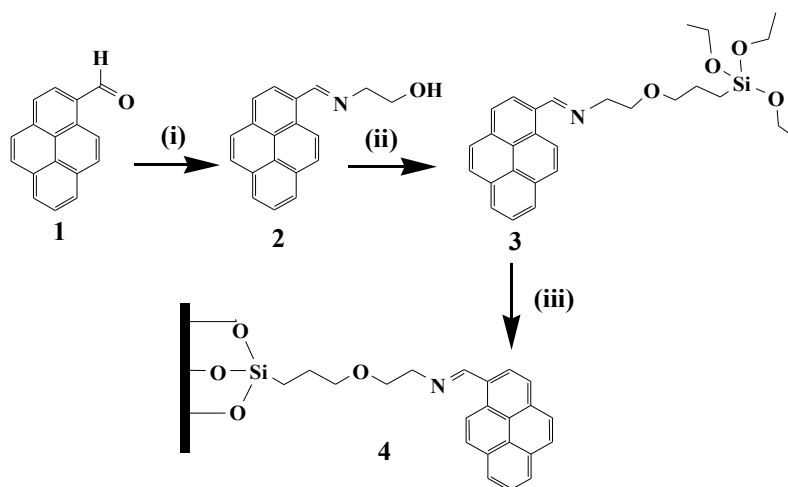
Scheme 1: (i) Ethanolamine/ethanol/reflux (ii) (3-chloropropyl)triethoxysilane /DIPEA/DCM (iii) Silica gel/dry DCM.
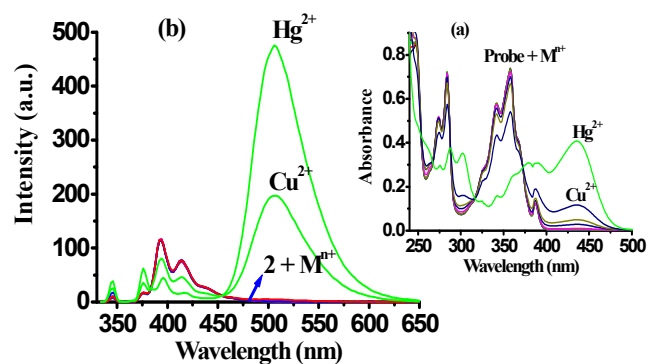
Figure 1: Change in (a) absorption and (b) emission spectra of **2** (10 μM) upon interaction with different metal ions (2.0 equiv) in phosphate buffer (10 mM pH 7.0; 10% aqueous ACN, v/v).
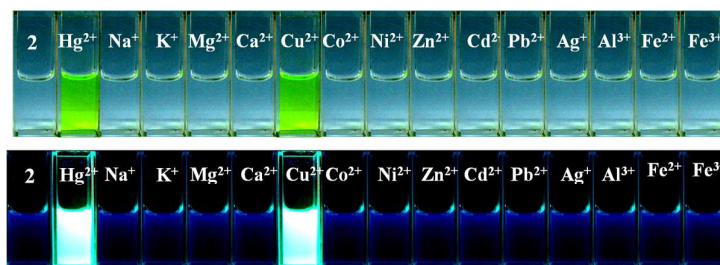
20

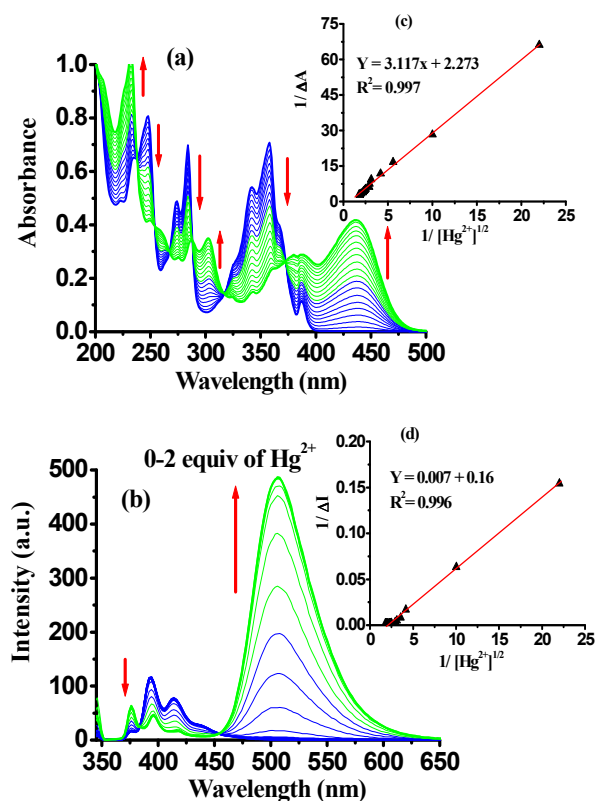**Figure 2:** Colorimetric and fluorogenic response of **2** (10 μM) upon interaction with different metal ions (2.0 equiv) in phosphate buffer (10 mM pH 7.0; 10% aqueous ACN v/v).

Figure 3: Change in (a) absorption and (b) emission titration spectra of **2** (10 μM) upon addition of Hg^{2+} (0-2 equiv) in phosphate buffer (10 mM pH 7.0; 10% aqueous ACN, v/v). Benesi-Hildebrand plots based (c) absorption and (d) emission titration data.
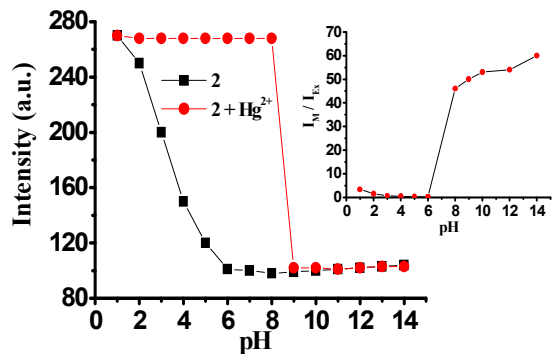
Figure 4: pH-emission plot exhibiting changes in relative fluorescence intensity of probe **2** and **2**+**Hg^{2+}** at different pH in phosphate buffer (10 mM; 10% aqueous ACN).
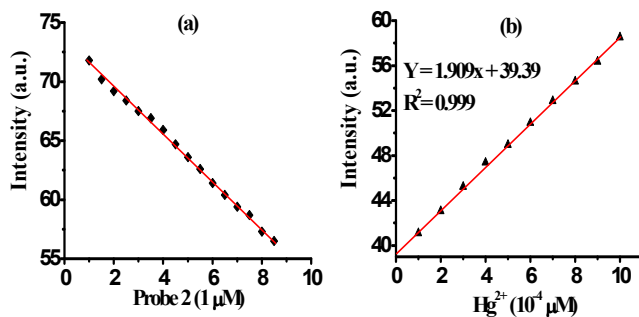
Figure 5: (a) Calibration curve between relative emission intensities and different concentration of probe **2** and (b) calibration sensitivity (m) plot for **2**+**Hg^{2+}**.

22
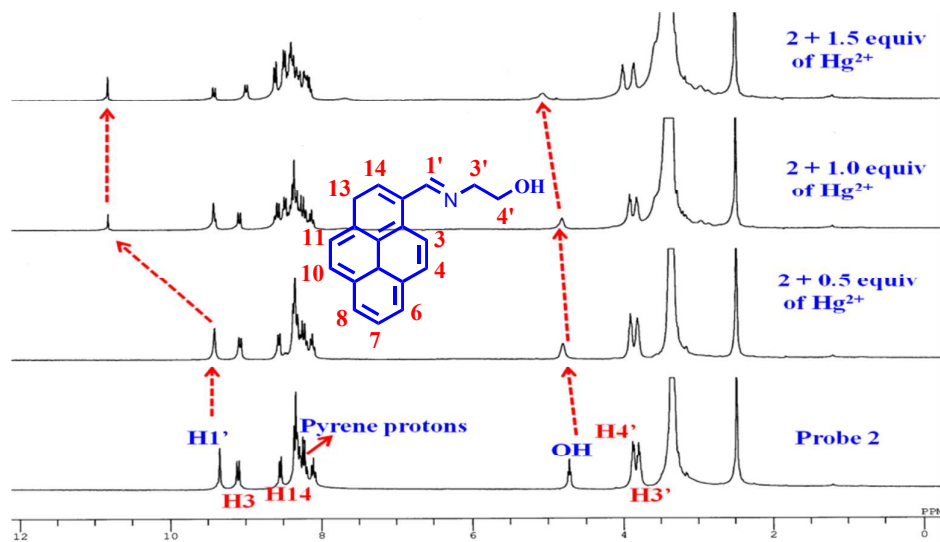
Figure 6: Change in ^{1}H NMR spectra of **2** (c = 1.02 x 10^{-2} M) upon addition of Hg^{2+} (0.5, 1and 1.5 equiv) in DMSO-d_6.
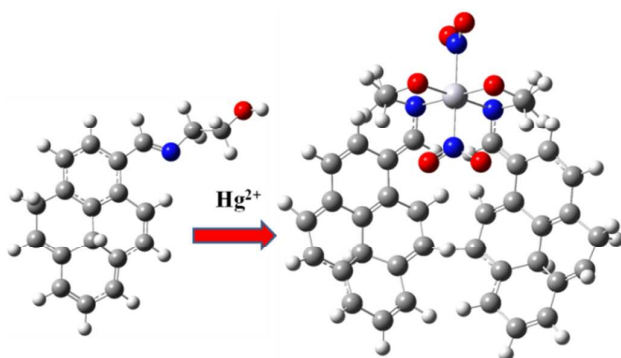
Figure 7: DFT optimized minimum energy structure of **2** and **2**-Hg^{2+} complex.

23
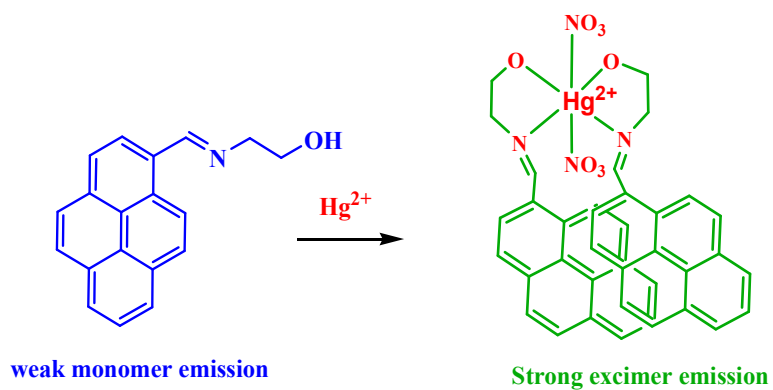
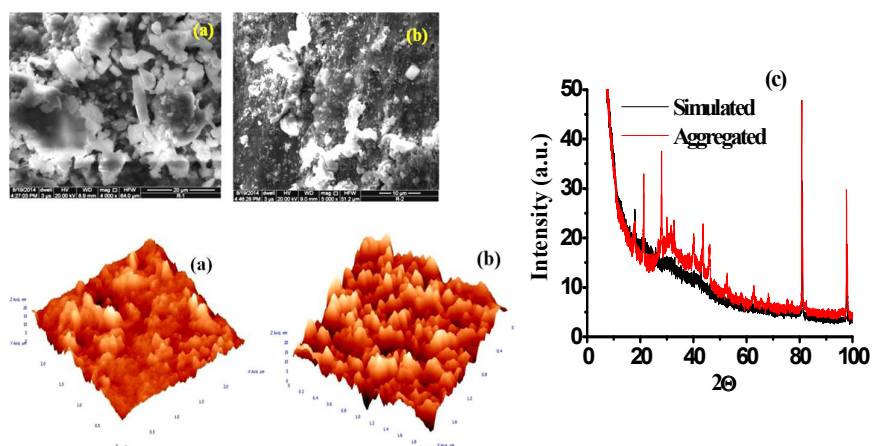**Scheme-2:** Proposed mechanism of interaction between **2** and Hg^{2+}.

Figure 8: SEM images of **4** (a) exhibiting crystalline, cylindrical, and spherical morphology with particle size 20 μm and (b) Hg^{2+} treated aggregated silica gel particles with particle size 10 μm. AFM 3D images show surface roughness of silica-gel particle **4** before (a) and after (b) Hg^{2+} treatment (c) Powder XRD pattern for **4** and **4**+Hg^{2+}.
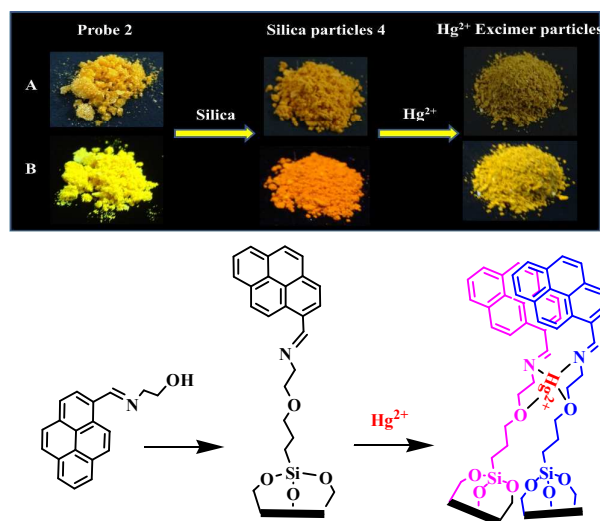
Figure 9: Images **(A)** Colorimetric **(B)** Fluorogenic color change of **2** and **4** upon interaction with Hg^{2+} in solid state, with plausible mode of interaction.
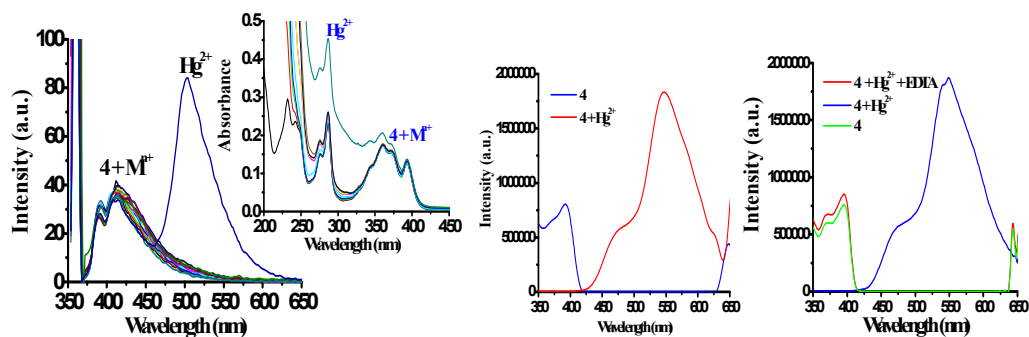

Figure 10: Change in absorption (inset) and emission spectra of sol solution of **4** (5 µM) upon interaction with different metal ions (2.0 equiv) in phosphate buffer (10 mM pH 7.0; 10% aqueous ACN, v/v). Change in solid state emission spectra of **4** upon interaction with Hg^{2+} and EDTA.
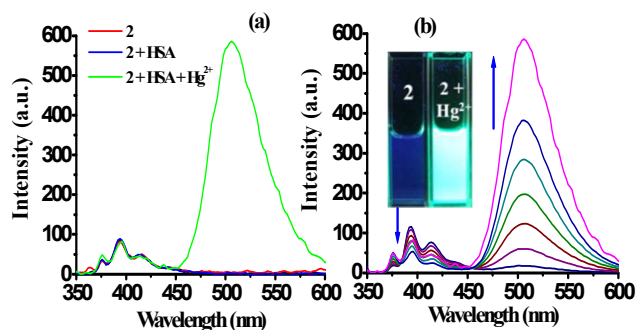
Figure 11: Changes in emission (a) and titration (b) spectra o**f 2** (10 µM probe; 2 µM HSA, pH 7.0) with Hg^{2+} (0-2 equiv) in phosphate buffer (10 mM pH 7.0; 10% aqueous ACN, v/v). Inset: color change after addition of Hg^{2+} in **2** containing human blood serum.
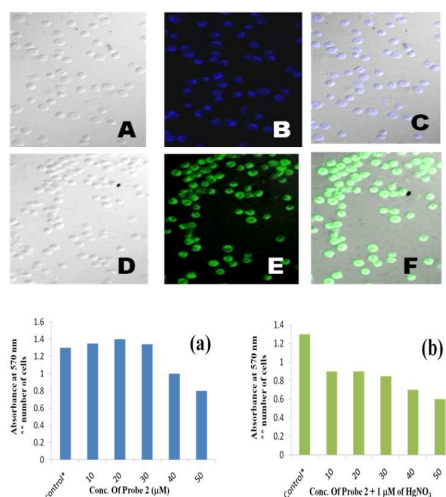

Figure 12. Confocal fluorescence images showing localization of **2** (blue in panel B) and **2**-Hg^{2+} (green in panel E) in the cytoplasm of live HeLa cells. DIC images of HeLa cells (panel A and D). Merged fluorescence images of probe **2** and **2**+Hg^{2+} (panel C and F). MTT assay histogram for (a) probe **2** and (b) **2**+$HgNO_3$.
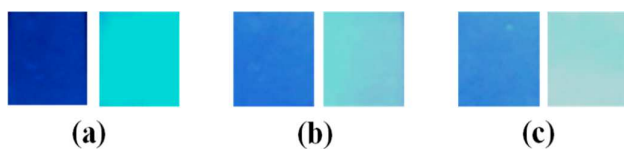
Figure 13: Fluorescent test paper strips of probe **2** (a) 5 µM, (b) 3 µM, (c) 1 µM before (blue) and after addition of Hg^{2+} (green) (a) 1×10^{-5}, (b) 1×10^{-7}, (c) 1×10^{-9} M under UV light at 365 nm.
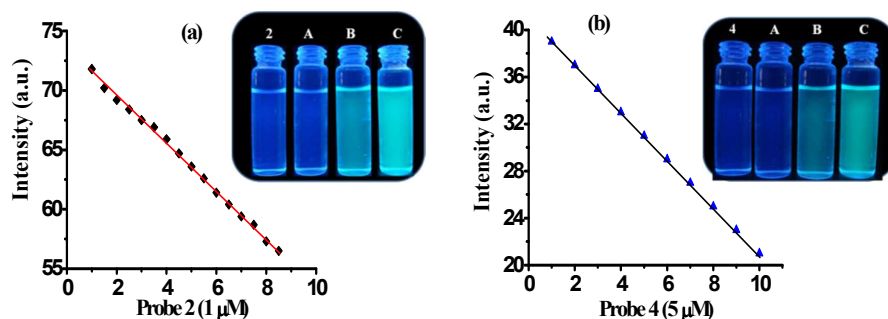

Figure 14: Calibration sensitivity plot of probe (a) **2** and (b) **4** toward Hg^{2+}. Inset: Change in color of probe **2** and **4** after treating with Hg^{2+} solution (A = 0.05, B = 0.5, C = 5 µM) in phosphate buffer (10 mM; pH 7.0; 10% aqueous ACN).

Table 1. Estimation of Hg^{2+} in water samples with probe 2

Sample concentration (μM)		Hg^{2+} recovered	% recovery of Hg^{2+} from the sample
Ganga River water	0	Not detected	-
	0.05	0.054± 0.014	108
	0.5	0.49 ± 0.021	98
	5	4.72 ± 0.18	94
Tap water	0	Not detected	-
	0.05	0.052± 0.014	104
	0.5	0.49 ± 0.021	98
	5	4.89 ± 0.22	98

Table 2. Estimation of Hg^{2+} in water samples with probe 4

Sample concentration (μM)		Hg^{2+} recovered	% recovery of Hg^{2+} from the sample
Ganga River water	0	Not detected	-
	0.05	0.058± 0.018	116
	0.5	0.48 ± 0.025	96
	5	4.82 ± 0.21	96
Tap water	0	Not detected	-
	0.05	0.056± 0.018	112
	0.5	0.46 ± 0.024	92
	5	4.88 ± 0.22	98

Only for TOC